ISSN 1063-7761, Journal of Experimental and Theoretical Physics, 2007, Vol. 105, No. 6, pp. 1141–1156. © Pleiades Publishing, Inc., 2007.
Original Russian Text © Yu.V. Senichev, A.N. Chechenin, 2007, published in Zhurnal Éksperimental'noĭ i Teoreticheskoĭ Fiziki, 2007, Vol. 132, No. 6, pp. 1302–1319.

## NUCLEI, PARTICLES, FIELDS, GRAVITATION, AND ASTROPHYSICS

# Construction of "Resonant" Magneto-Optical Lattices with Controlled Momentum Compaction Factor

**Yu. V. Senichev[a] and A. N. Chechenin[b]**

[a] *Institute of Nuclear Physics, FZJ, D-52428, Jülich, D-52425, Jülich, Germany*
*e-mail: y.senichev@fz-juelich.de*
*Institute of Nuclear Research, Russian Academy of Sciences, Moscow, 117312 Russia*
[b] *St. Petersburg State University, St. Petersburg, 199034 Russia*
*e-mail: a.chechenin@fz-juelich.de*

Received July 31, 2007

**Abstract**—On the basis of the theory of "resonant" magneto-optical lattices for synchrotrons with complex transition energy developed in [1], methods for construction of such lattices with application to various accelerators are proposed. Apart from allowing elimination of transition energy crossing by accelerated particles, these lattices should meet a number of important requirements. In particular, they must have dispersion-free straight sections intended for accommodation of RF cavities, Siberian snakes and detectors, and a large enough dynamic aperture for minimizing the effect of magnetic optics nonlinearity on the beam parameters after chromaticity correction by sextupoles.

PACS numbers: 29.20.Lq, 29.27.-a, 29.27.Bd, 45.20.Jj

**DOI:** 10.1134/S1063776107120060

## 1. INTRODUCTION

With special modulation of lens gradients and orbit curvature and a particular choice of betatron oscillation frequencies, the theory of resonant magneto-optical lattices developed in [1] makes it possible to obtain interrelated dispersion variations of $D(s)$ and orbit curvature $1/\rho(s)$ along the equilibrium orbit $s$ and a negative momentum compaction factor

$$\alpha = \frac{1}{C}\oint^{C}\frac{D(s)}{\rho(s)}ds \le 0. \quad (1)$$

A lattice with negative $\alpha$ precludes transition energy crossing by accelerated particles since the transition energy takes complex values $\gamma_{tr} = -i/\sqrt{|\alpha|}$. In addition, the lattice must meet a number of physical and technical requirements, such as independent tuning of the momentum compaction factor and betatron frequencies of arks, zero dispersion in straight sections, effective chromaticity correction by the smallest possible number of quadrupole families, and a large dynamic aperture. The latter implies, first of all, mutual compensation of the nonlinear effect of chromatic sextupoles on the motion of particles in the accelerator in the first order of perturbation theory.

In this paper we propose methods for construction of magneto-optical lattices complying with the above conditions and discuss which lattice is optimal in view of the possible technological features of a particular accelerator. All numerical results mainly apply to the project of the antiproton high-energy storage ring (HESR) to be implemented within the international FAIR (Facility for Antiproton and Ion Research) project in Darmstadt (Germany) [2, 3] in which the authors take part. However, the results obtained in this study may be used for any similar accelerator of energy ranging from 1 to 100 GeV.

The resonant magneto-optical lattice was first proposed for the Moscow Kaon Factory [4]. This lattice was then adapted for the TRIUMF KAON Factory (Canada) [5, 6]. Later it was considered the best lattice for the Superconducting Super Collider (SSC) Booster (United States) [7], then was adopted for the main accelerator of the Neutrino Factory at CERN (Switzerland) [8], and ultimately was implemented in the J-PARC (Japan Proton Accelerator Research Center) accelerator complex [9, 10].

## 2. GENERAL APPROACH TO THE CONSTRUCTION OF THE RESONANT LATTICE

General principles of construction of resonant lattices detailed in [1] are based on the solution of the equation for the dispersion $D(s)$ in the biperiodical structure

$$\frac{d^2D}{ds^2} + [K(s) + \varepsilon k(s)]D = \frac{1}{\rho(s)}. \quad (2)$$

Here, the gradient $G(s)$ and the orbit curvature $1/\rho(s)$, related to each other by means of the functions

$$K(s) = \frac{eG(s)}{p}, \quad \varepsilon k(s) = \frac{e\Delta G(s)}{p},$$

where $p = m_0\gamma v$ is the particle momentum, should be modulated resonantly and in correlation with each other.

In what follows we will use the harmonics of the modulated function of gradients

$$\varepsilon k(\phi) = \sum_{k=0}^{\infty} g_k \cos k\phi, \tag{3}$$

where

$$g_k = \frac{e}{p}\frac{1}{\pi}\int_{-\pi}^{\pi} \Delta G \cos k\phi d\phi$$

is the $k$th Fourier harmonic of the gradient function and

$$\phi = 2\pi\frac{s}{L_s}$$

is the longitudinal coordinate normalized to the superperiod length $L_s$, and the harmonics in the expansion of the curvature function

$$\frac{1}{\rho(\phi)} = \frac{1}{\bar{R}}\left(1 + \sum_{n=1}^{\infty} r_n \cos n\phi\right), \tag{4}$$

where

$$r_n = \frac{\bar{R}}{\pi}\int_{\pi}^{-\pi} \frac{\cos n\phi}{\rho(\phi)} d\phi$$

is the $n$th Fourier harmonic of the orbit curvature and

$$\bar{R} = L_s\frac{S}{2\pi}$$

is the mean curvature radius of the equilibrium orbit in the superperiod, where $S$ is the number of superperiods.

Since mirror symmetry of the superperiod is one of the conditions for the construction of the resonant lattice, expansions of the functions $\varepsilon k(\phi)$ and $1/\rho(\phi)$ in Fourier series involve only terms with cosines.

According to (1), the momentum compaction factor is the average value of the function $D(\phi)/\rho(\phi)$. In the general form, the dispersion $D(\phi)$ and the orbit curvature $1/\rho(\phi)$ can be represented in terms of the averages $\bar{D}$ and $\bar{R}$ and the functions $\tilde{D}(\phi)$, $\tilde{r}(\phi)/\bar{R}$ oscillating about these averages. Then the momentum compaction factor can be written as the sum

$$\alpha = \frac{\bar{D}}{\bar{R}} + \frac{\overline{\tilde{D}(\phi)\tilde{r}(\phi)}}{\bar{R}}. \tag{5}$$

In an ordinary lattice without gradient and orbit curvature modulation, the oscillating components vanish, $\tilde{D}(\phi) = 0$, $\tilde{r}(\phi) = 0$, and the momentum compaction factor is governed by the first term in (5). Considering that the average dispersion in classical lattices is

$$\bar{D} = \frac{\bar{R}}{\nu^2},$$

we find that the minimum value of the momentum compaction factor

$$\alpha = \frac{\bar{D}}{\bar{R}} = \frac{1}{\nu^2}$$

is limited by the total number of horizontal betatron oscillations $\nu$ in the magneto-optical lattice of length $SL_s$. In the resonant lattice, the functions of gradients and/or orbit curvature can be modulated jointly or individually. In [1] general expressions were obtained for the momentum compaction factor for one superperiod,

$$\begin{aligned}\alpha_s = \frac{1}{\nu^2}\Bigg\{1 + \frac{1}{4}\left(\frac{\bar{R}}{\nu}\right)^4 \sum_{k=-\infty}^{\infty} \\ \times \frac{g_k^2}{(1-kS/\nu)[1-(1-kS/\nu)^2]} + \frac{1}{4}\sum_{k=-\infty}^{\infty}\frac{r_k^2}{1-kS/\nu} \\ -\frac{1}{2}\left(\frac{\bar{R}}{\nu}\right)^2 \sum_{k=-\infty}^{\infty}\frac{r_k g_k}{(1-kS/\nu)[1-(1-kS/\nu)^2]} \\ -\frac{1}{2}\left(\frac{\bar{R}}{\nu}\right)^2 \sum_{k=-\infty}^{\infty}\frac{r_k g_k}{1-(1-kS/\nu)^2} \\ + O(g_k^i, r_k^j, i+j \geq 3)\Bigg\},\end{aligned} \tag{6}$$

and for the dispersion function maximum in a superperiod,

$$\begin{aligned}D_{\max} = \frac{\bar{R}}{\nu^2}\hat{f} \\ \times\Bigg\{1 - \frac{1}{2}\left(\frac{\bar{R}}{\nu}\right)^2 \sum_{k=-\infty}^{\infty}\frac{g_k}{(1-kS/\nu)[1-(1-kS/\nu)^2]} \\ -\frac{1}{2}\left(\frac{\bar{R}}{\nu}\right)^2 \sum_{k=-\infty}^{\infty}\frac{g_k}{1-(1-kS/\nu)^2} \\ + \frac{1}{2}\sum_{k=-\infty}^{\infty}\frac{r_k}{1-kS/\nu} + O(g_k^i, r_k^j, i+j \geq 2)\Bigg\},\end{aligned} \tag{7}$$

where $kS$ is the modulation frequency of the $k$th harmonic in the expansion of the gradient and curvature

functions, and $\hat{f}$ is a function describing beam envelope oscillations, which is normalized to its average value. We will call the harmonic closest to $\nu$ (with the minimum possible difference $kS - \nu$) and producing the maximum effect on the momentum compaction factor the fundamental harmonic. This harmonic has $kS$ oscillations over the entire lattice in question. In most cases under our consideration the frequency of the $k$th harmonic coincides with the number of superperiods, i.e., $k = 1$ and $kS = S$. Indeed, if both the lens gradient function and the orbit curvature function are modulated with an identical frequency (i.e., at $k = n$ in (3) and (4)), the second term in (5) may make an appreciable contribution to the momentum compaction factor provided that the value $1 - kS/\nu$ is small (see (6)). In addition, from (7) there follows an obvious condition of antiphase modulation of the gradient and curvature function, which allows correlated variation of the momentum compaction factor with the aid of these functions. We call this lattice, based on the resonant and correlated perturbation of the magneto-optical channel parameters, the resonant lattice.

Thus, the following principles underlie the general approach to construction of a resonant lattice:

(i) the fundamental modulation frequency should be identical for the functions of the gradients and the orbit curvature and higher than the horizontal betatron frequency $kS > \nu$ with as small a difference $kS - \nu$ as possible;

(ii) modulation of the orbit curvature should be in antiphase with modulation of the lens gradients, $g_k r_k < 0$;

(iii) amplitudes of each of the fundamental harmonics, $g_k$ and $r_k$, should be as high as possible;

(iv) exact equality of the frequencies $\nu = kS$ and $\nu = kS/2$ at which the dispersion and the $\beta$-function increase beyond limits should be eliminated.

## 3. A SUPERPERIOD OF THE RESONANT LATTICE

There are two types of lattices used in accelerators with inserted straight sections, the so-called circular lattices with $S$ identical superperiods and the lattice consisting of arcs with $S$ superperiods separated by straight sections. In the former lattices the momentum compaction factor completely coincides with its value for one superperiod. In the lattices consisting of arcs with a total of $S$ superperiods separated by straight sections of length $L_{\text{str}}$, the momentum compaction factor for the entire accelerator $\alpha$ and for a superperiod $\alpha_s$ are related by the equation

$$\alpha = \alpha_s \frac{SL_s}{SL_s + L_{\text{str}}}.$$

Thus, knowing the momentum compaction factor for one superperiod, one can easily find its value for the entire accelerator. A superperiod is usually formed by varying parameters of a regular lattice consisting of singlet FODO cells, doublet FDO cells, or triplet FDFO cells (F is the focusing quadrupole, D is the defocusing quadrupole, and O is the drift space), each having its advantages and drawbacks. However, considering the chromaticity compensation requirement, the FODO lattice is most preferable because the other two lack good separation of the horizontal and vertical $\beta$ functions, which results in a decreased efficiency of the sextupoles and accordingly in a decreased dynamic aperture. In addition, the FODO superperiod with mirror symmetry about its center provides most favorable conditions for independent control of the betatron frequencies, chromaticity in both planes, and momentum compaction factor, which makes a lattice like this superior to any other.

The number of cells in a superperiod $N_{\text{cell}}$ is dictated by the required phase advance of radial oscillations. Following the theory of resonant lattices, we will try to construct a lattice with the horizontal frequency $\nu$ as close to the number of superperiods as possible [1]. In this case, the phase advance of radial oscillations per cell will be about $2\pi\nu/SN_{\text{cell}}$. At the same time it is known that from the point of view of minimization of the $\beta$-functions for a cell the phase advance of radial oscillations should fall within the range 60°–100°. Thus, in a lattice with the fundamental harmonic of the modulation of the superperiod parameters $k = 1$ and with $\nu < S$, the number of cells turns out to be 3–5 per superperiod.

Since an increase in the number of cells requires greater splitting of the superperiod and entails an increase in the number of magneto-optical elements, we exclude the five-cell option from consideration and confine ourselves to analysis of a superperiod comprising 3–4 cells. Figures 1a–1f correspond to various versions of superperiods used in resonant lattices. According to the theory of resonant structures, either modulation of the lens gradients or modulation of the orbit curvature, or simultaneous modulation of both functions is introduced to get the required momentum compaction factor $\alpha$ [1].

Figure 1a shows the behavior of the function $\beta_{x,y}$ and $D_x$ in a channel of three FODO cells, where each drift space accommodates a bending magnet. It is more appropriate to call this structure an FBDB cell (B is the bending magnet). Obviously, strict periodicity of cells does not make it possible to get the required value of the momentum compaction factor, which is fixed by the value of the horizontal betatron frequency in this case.

Figure 1b shows a superperiod made up of three FDBD cells with gradient modulation alone and mirror symmetry about the center, where two quadrupole families form the required fundamental harmonic $k = 1$. However, this modulation method requires a great change of field in the lenses. Note that strong modulation of the gradients leads to a considerable increase in $\beta$-functions and chromaticity of the entire accelerator, which results in a reduced dynamic aperture; therefore,

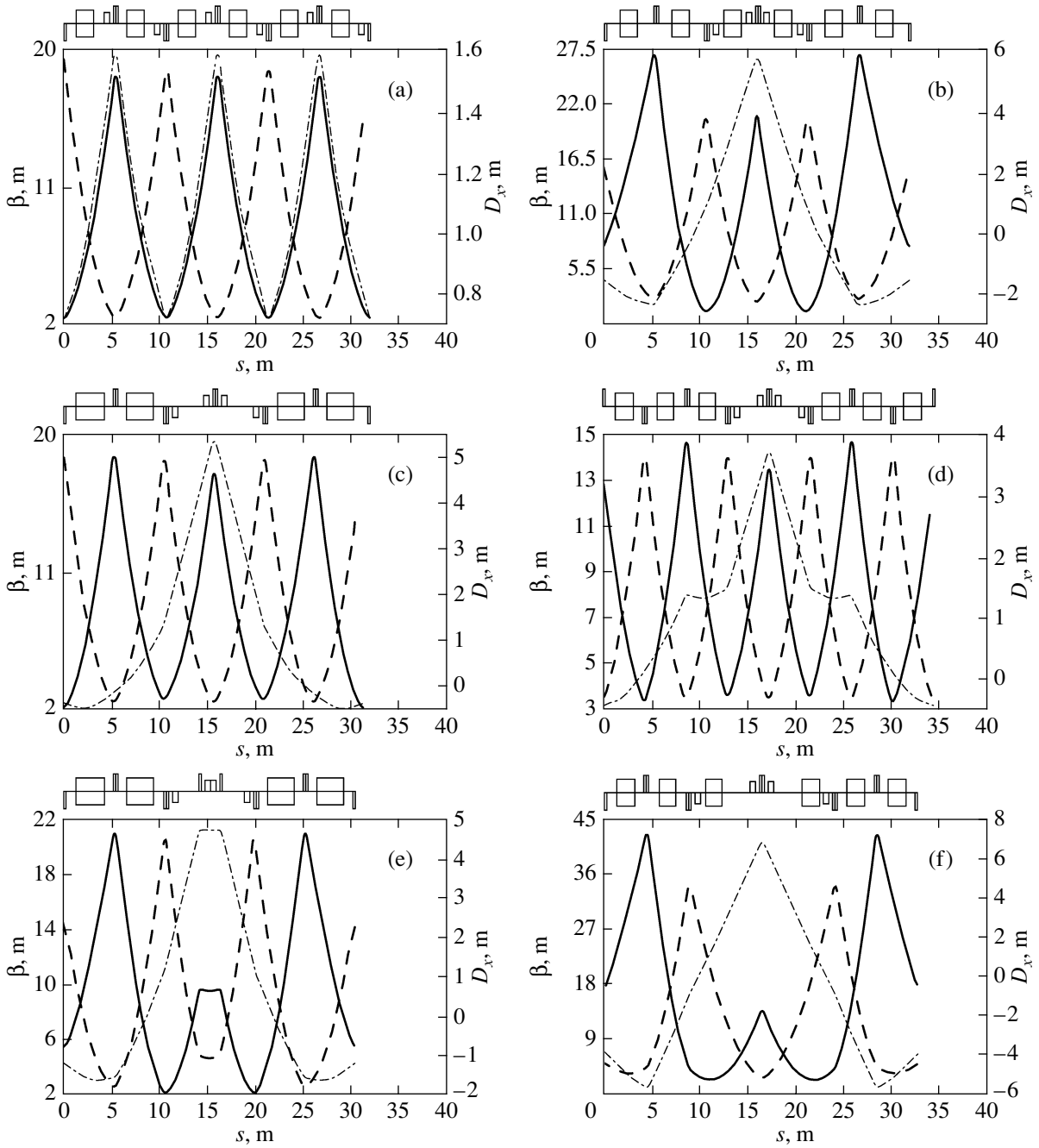


**Fig. 1.** Dependence of the $\beta_x$-function (solid curves), $\beta_y$-function (dashed curves), and $D_x$ (dot-dashed curves) on the distance $s$ over the accelerator channel for the magneto-optical channel of three regular cells (a); the three-cell superperiod with lens gradient modulation (b); the three-cell superperiod with orbit curvature modulation (c); the four-cell superperiod with orbit curvature modulation (d); the three-cell superperiod with the central quadrupole sliced (e); and the three-cell superperiod with six magnets (f).

this version of the resonant lattice is not considered below.

Figures 1c and 1d correspond to the lattices where a superperiod is made up of three and four cells respectively and the fundamental harmonic $k = 1$ is produced by modulation of the orbit curvature through using empty central cells called missing magnets (or missing magnet cells) [11, 12]. In these curvature-varying lattices, β-functions remain practically unperturbed and chromaticity is kept at a level corresponding to the periodical optics. Unfortunately, the orbit curvature modulation method does not always provide the required momentum compaction factor. Figures 1e and 1f show the results yielded by various modifications of the method. In the first case (Fig. 1e), the central quadrupole is "cut" in two slices and a sextupole is inserted between the slices, as was done, for example, in the J-PARC project [10]. On the one hand, positioning of

the sextupole at a point where the horizontal β-function has a large value increases its efficiency and thus the total number of focusing sextupoles can be reduced. On the other hand, division of a quadrupole into two halves increases their number. To our mind, this design does not give any significant advantages and is only a modification of the universally accepted resonant lattice. In the second case (Fig. 1f), the orbit curvature is varied without a decrease in the total number of magnets, by varying the central cell length alone. This option may be advantageous for a magneto-optical lattice with rectangular magnets because the magnet sagitta is considerably decreased.

In the following sections we consider various approaches to the momentum compaction factor control by separated and combined modulation of the curvature function and the function of the gradients in the magnetic lenses. We show that the latter approach is preferable.

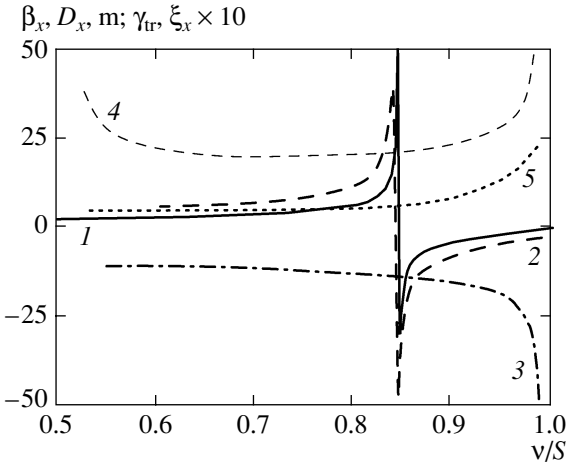


**Fig. 2.** Dependence of the transition energy $\gamma_{tr}$ (*1* is analytical calculation, *2* is MAD calculation) and the functions $\xi_x$ (*3* calculation by MAD), $\beta_x$ (*4* calculation by MAD), and $D_x$ (*5* calculation by MAD) on $\nu/S$ for the three-cell superperiod with the modulated orbit curvature function.

## 4. MODULATION OF THE ORBIT CURVATURE FUNCTION

Let us consider a lattice where the orbit curvature $1/\rho$ and the lens gradients $\Delta G$ are modulated separately. We begin with the case where only $1/\rho$ is modulated.

On the one hand, modulation of the orbit curvature requires magnet-free space, which leads to an increase in the total length (perimeter) of the accelerator. On the other hand, the free space concentrated in one place can be used more effectively, which allows, conversely, a decrease in the total length (perimeter) of the accelerator. For example, sextupoles, multipole correctors, diagnostics and vacuum equipment, uniformly distributed over the entire orbit in the previous design, can now be arranged in a more compact way in the free central part of the superperiod. As far as the efficiency of the chromaticity compensation by sextupole lenses is concerned, resonant lattices with $\nu < S$ have an important feature, namely, the dispersion oscillating in antiphase with the orbit curvature achieves its maximum in sections of zero curvature, $1/\rho = 0$ (see Figs. 1c–1f). Consequently, the sextupoles located in these sections are at the points corresponding to the dispersion maximum. In addition, the missing magnet cell can be simultaneously used for both sextupole families because the $\beta_x$- and $\beta_y$-functions are well separated within this cell. Both facts to a large extent allow preserving the dynamic aperture. At the same time the dispersion in the bending magnets will be lower than in the regular structure (see Figs. 1a, 1c), which reduces the physical aperture of the magnet. This all applies to multipole correctors as well since their efficiency also depends on the dispersion value at their locations. The missing magnet cell is also suited to accommodate diagnostic equipment.

If we compare three-cell and four-cell superperiods (Figs. 1c, 1d), we find that in the former case the orbit curvature modulation is more effective from the point of view of the desired momentum compaction factor because the three-cell structure with its larger ratio of missing magnet cells to the total number of cells has a larger fundamental harmonic value $r_k$. Certainly, the four-cell structure also allows the fundamental harmonic value to be increased by inserting an additional missing magnet cell, but this will cause an unjustified increase in the perimeter of the accelerator. Therefore, the lattice based on the three-cell superperiod is preferable.

Figure 2 shows the results of calculating the dependence of the transition energy $\gamma_{tr}$, horizontal $\beta_x$-function, horizontal dispersion $D_x$, and chromaticity normalized to $\nu$

$$\xi_x = \frac{1}{\nu}\frac{d\nu}{d\delta}$$

on the horizontal betatron frequency $\nu$ normalized to the number of superperiods $S$ for a three-cell superperiod ($\delta = \Delta p/p$ is the relative momentum spread). The calculations were performed with the programs MAD [13] and OptiM [14]. For the transition energy $\gamma_{tr}$, a dependence obtained analytically by formula (6) is also constructed. At a certain value of the horizontal frequency $\nu = \nu_{tr}$ the momentum compaction factor $\alpha = 1/\gamma_{tr}^2$ reverses its sign from positive to negative and the transition energy becomes complex. As is evident from Fig. 2, the transition occurs by a jump. At the point where the momentum compaction factor $\alpha$ passes through zero and in going further into the region of its negative values, the values of $\beta_x$, $D_x$, and $\xi_x$ are not large. However, as one approaches the point $\nu = S$, the values of these functions increase indefinitely, demonstrating typical parameter instability.

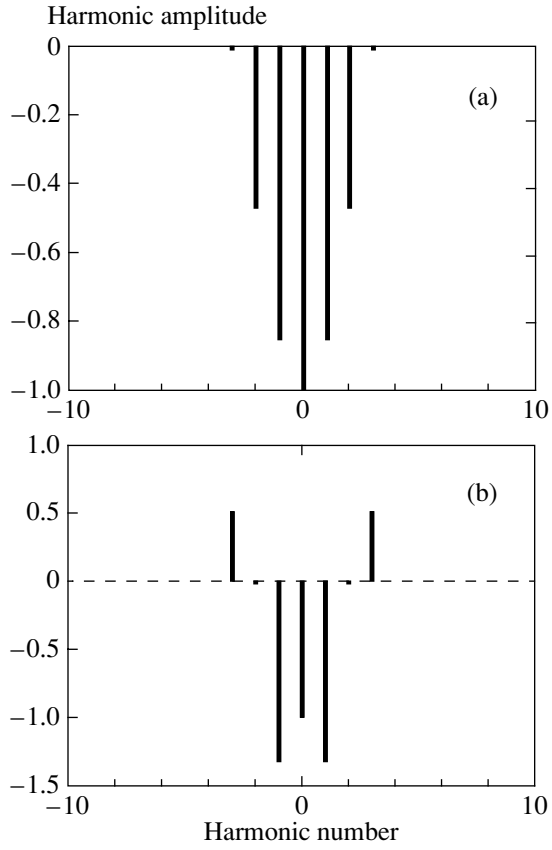


**Fig. 3.** Fourier harmonic spectrum of the modulated orbit curvature function for the superperiod with the regular missing magnet cell (a) and the twice as long one (b).

In resonant structures, the frequency range from $\nu = \nu_{tr}$ to $\nu = S$ is most important for us because we are interested in having a negative momentum compaction factor together with motion stability and tolerable values of beam parameters. The distance between the points $\nu = \nu_{tr}$ and $\nu = S$ is dictated by the lattice properties, namely, by the value of the fundamental perturbation harmonic.

Figure 3 shows Fourier harmonic spectra of the orbit curvature function for a superperiod with all cells of the same length (a) and with the missing magnet cell twice as long (b). In the case of centrally located missing magnet cells of the superperiod, the fundamental and neighboring Fourier harmonics have large negative values in both figures. As we see, in the latter case (Fig. 3b), the fundamental harmonic $k = 1$ has a larger value because the missing magnet cell is twice as long. Note that the $k = 2$ harmonic closest to the fundamental harmonic in Fig. 3a has a larger value, but it hardly affects the momentum compaction factor because of "attenuation" of the factor $1/(1 - kS/\nu)$.

For $k = 1$, simple expressions for the momentum compaction factor and the maximum dispersion can be easily obtained from (6) and (7) with $g_k = 0$:

$$\alpha_s = \frac{1}{\nu^2}\left[1 + \frac{1}{4}\frac{r_1^2}{1 - S/\nu}\right], \tag{8}$$

$$D_{\max}(\phi) = \frac{\bar{R}}{\nu^2}\hat{f}\left[1 + \frac{1}{2}\frac{r_1}{1 - S/\nu}\right]. \tag{9}$$

It is evident from (8) that a lattice with the fundamental harmonic

$$r_1 = \pm 2\sqrt{\frac{S}{\nu_{tr}} - 1} \quad \text{or} \quad \nu_{tr} = \frac{S}{1 + r_1^2/4}, \tag{10}$$

is necessary for having a zero momentum compaction factor $\alpha_s = 0$. According to (10) that the closer the frequency to the parametric resonance value $\nu = S$, the smaller the fundamental harmonic $r_1$ is required; and vice versa, the larger the amplitude of the fundamental harmonic, the farther the detuning from the resonance at which zero momentum compaction factor can be obtained. The plus sign in (10) means that the missing magnet half-cells are placed at the ends of the superperiod, while the minus sign means that the missing magnet cell is located at the center of the superperiod. The latter option is more preferable because fundamental harmonics must be of opposite sign for the combined effect of the gradient and orbit curvature modulations.

To verify the resonant theory developed in [1], dependence of the transition energy on the frequency of horizontal betatron oscillations was constructed for a particular fundamental harmonic $r_1 = 0.86$ (see Fig. 2). A comparison of the results obtained by (6) and the numerical results obtained with the MAD code demonstrates quite good qualitative agreement of the behavior of both curves and almost exact coincidence of the points where the transition energy $\gamma_{tr}$ enters the region of complex values: $\nu_{tr} = 3.37$ (by (6)) and $\nu_{tr} = 3.38$ (by MAD) (see Fig. 2).

Let us evaluate the maximum value of the dispersion at the point $\nu_{tr} \approx 3.38$. Considering the central position of the missing magnet cell, from (9) and (10) we get

$$D_{\max} = \hat{f}_{\max}\frac{\bar{R}}{\nu_{tr}^2}\left[1 + \frac{1}{\sqrt{S/\nu_{tr} - 1}}\right]. \tag{11}$$

A comparison of the values $D_{\max}^{\text{mod}}$ for a superperiod with the modulated orbit curvature and $D_{\max}^{\text{reg}}$ in a regular modulation-free lattice calculated by (11) yields

$$\frac{D_{\max}^{\text{mod}}}{D_{\max}^{\text{reg}}} \approx 3.33.$$

This ratio is governed by the bracketed quantity in (11). It can be found by numerical calculations using the MAD code (see Figs. 1a and 1c), and the result coincides with the analytical one to a high accuracy. This indicates that the resonant theory [1] describes well the

main properties of the lattice with orbit curvature modulation.

It is easy to show that in the general case, where the ratio between the number of missing magnet cells and the total number of cells is equal to $K$, the fundamental harmonic is defined by the expression

$$r_k = -\frac{2\sin(\pi kK)}{\pi k}\frac{1}{1-K}. \quad (12)$$

The minus sign in (12) corresponds, as above, to the location of the missing magnet cell at the center of the superperiod. Taking into account only one fundamental harmonics and substituting its value into (6) and (7), we get expressions similar to (8) and (9),

$$\alpha_s = \frac{1}{\nu^2}\left[1 + \frac{\sin^2(k\pi K)}{k^2\pi^2}\left(\frac{1}{1-K}\right)^2\frac{1}{1-kS/\nu}\right] \quad (13)$$

and

$$D_{\max} = \hat{f}_{\max}\frac{\bar{R}}{\nu^2}\left[1 + \frac{1}{2}\frac{\dfrac{\sin(k\pi K)}{\pi k}\left(\dfrac{1}{1-K}\right)}{1-kS/\nu}\right]. \quad (14)$$

When $K \geq 0.4$, the fundamental harmonic $r_k \geq 1$; when $K \longrightarrow 1$, $r_k \longrightarrow 2$. This means that one can obtain almost any momentum compaction factor by orbit curvature modulation alone, without being restricted to a particular orbit length or phase advance of radial oscillations.

As an example of how the orbit curvature modulation allows elimination of transition energy crossing, we consider the proton synchrotron at the KEK National Laboratory (Japan) [15], built about 40 years ago. The structure of one of four lattice superperiods of the accelerator is shown in Fig. 4a. The total energy of the accelerator is 12 GeV and the particles under acceleration cross the transition energy at 5.4 GeV, which is the major obstacle to an increase in the intensity of the accelerated beam. Each superperiod consists of seven FODO cells and is not mirror symmetrical. The superperiodicity is formed by two drift spaces at the beginning of each superperiod. The betatron frequency in the horizontal plane is $\nu = 7.25$ over the entire ring. To increase the transition energy and thus to eliminate its crossing in the course of acceleration, the lattice should be modified in the resonant way. One of the possible ways is to introduce a twice as long superperiodicity; i.e., eight instead of four superperiods are formed over the magnets in the entire accelerator. This results in excitation of the fundamental harmonic ($k = 1$) of the orbit curvature modulation over the length of 3.5 cells with simultaneous tuning of the horizontal betatron frequency to $\nu = 0.85$ in the new superperiod as long as 1/8 of the ring. Figure 4b shows behavior of the β-functions and dispersion in the modified structure over the length of two new superperiods. This resonant method allows quite easy elimination of transition energy crossing.

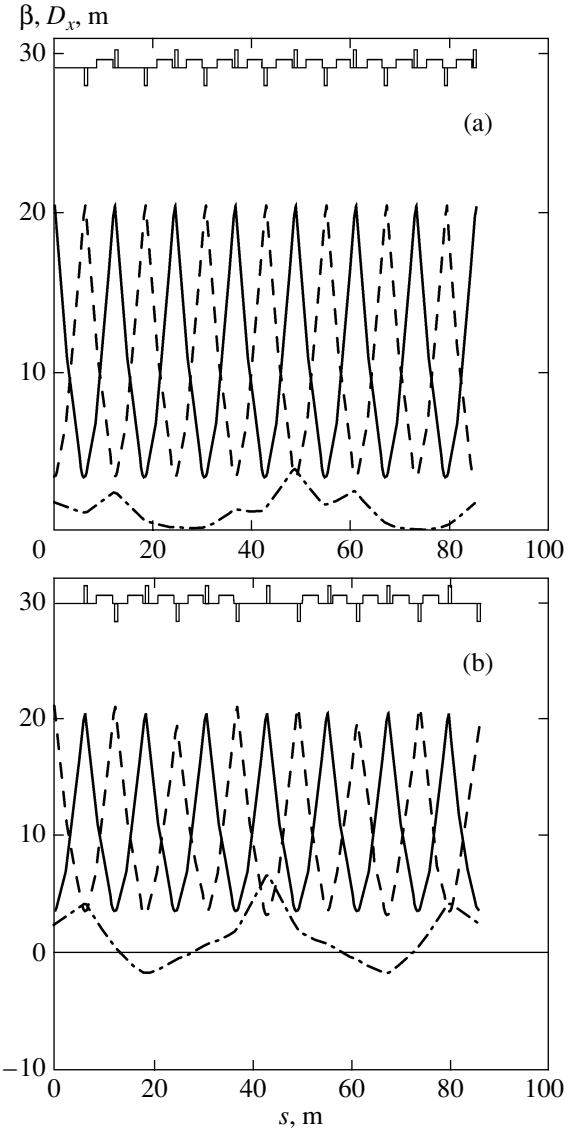


**Fig. 4.** (a) Lattice of the KEK proton synchrotron: one superperiod (horizontal betatron frequency in the ring $\nu = 4 \times 1.8125$); (b) the modified KEK lattice: two superperiods with orbit curvature variation (horizontal betatron frequency in the ring $\nu = 4 \times 1.7$); designations of the curves are the same as in Fig. 1.

However, it requires an additional missing magnet cell, which leads to a 20% increase in the magnetic fields of the remaining magnets. This method hardly disturbs the β-functions and the dispersion increases only in the drift spaces. Note also that this method can be successfully implemented only with a quite close approach to the parametric resonance point, which entails an increase in dispersion.

## 5. MODULATION OF THE LENS GRADIENT FUNCTION

Now let us consider the case where only gradients in lenses are modulated, i.e., $r_k = 0$. From general expres-

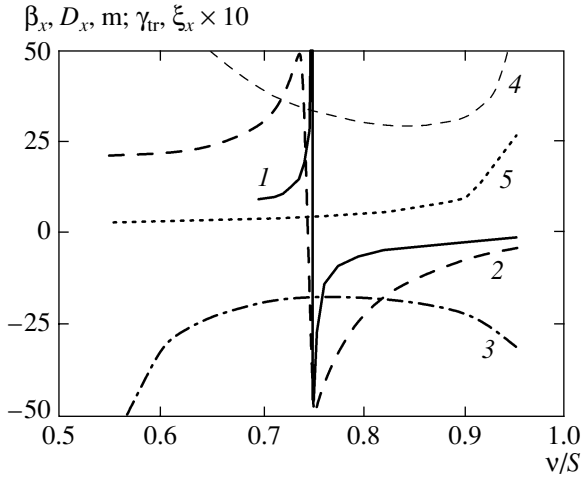


**Fig. 5.** Dependence of the transition energy $\gamma_{tr}$ (analytical calculation *1*, MAD calculation *2*) and the functions $\xi_x$ (MAD calculation *3*), $\beta_x$ (MAD calculation *4*), $D_x$ (MAD calculation *5*) on $\nu/S$ for the three-cell superperiod with the modulated gradient function.

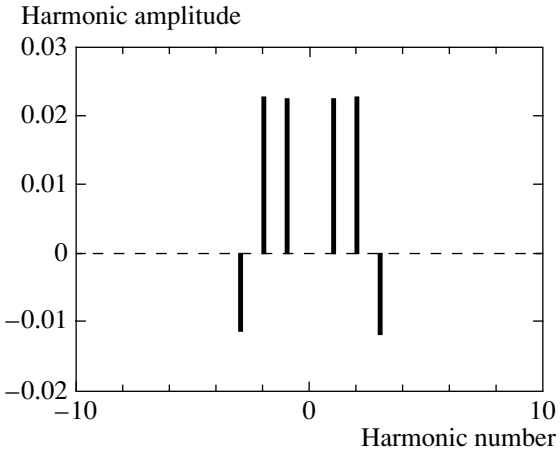


**Fig. 6.** Fourier harmonic spectrum of the modulated lens gradient function for the three-cell superperiod.

sions (6) and (7) it is easy to derive formulas for the momentum compaction factor and the maximum dispersion corresponding to one fundamental harmonic of the gradient function modulation at $r_k = 0$:

$$\alpha_s = \frac{1}{\nu^2}\left\{1 + \frac{1}{4(1-kS/\nu)}\left(\frac{\bar{R}}{\nu}\right)^4 \times \frac{g_k^2}{[1-(1-kS/\nu)^2]^2}\right\}, \quad (15)$$

$$D_{\max} = \frac{\bar{R}}{\nu^2}\hat{f}\left\{1 - \frac{1}{2(1-kS/\nu)}\left(\frac{\bar{R}}{\nu}\right)^2 \times \frac{g_k}{1-(1-kS/\nu)^2}\right\}. \quad (16)$$

It follows from (15) that $\alpha = 0$ at the fundamental harmonic amplitude

$$g_k = \pm 2\sqrt{\frac{kS}{\nu_{tr}} - 1}\left(\frac{\nu_{tr}}{\bar{R}}\right)^2\left[1 - \left(1 - \frac{kS}{\nu_{tr}}\right)^2\right]. \quad (17)$$

It is evident from (17) (as in previous section) that the closer the horizontal betatron frequency $\nu$ to the frequency of the fundamental harmonic of gradient modulation $kS$, the smaller the fundamental harmonic amplitude $g_k$ should be, and vice versa. From (16), in view of (17) taken with the plus sign, we get the expression for the maximum dispersion

$$D_{\max} = \frac{\bar{R}}{\nu_{tr}^2}\hat{f}\left\{1 + \frac{1}{\sqrt{kS/\nu_{tr} - 1}}\right\}. \quad (18)$$

In the case of a three-cell superperiod, the required modulation $g_k$ is provided by two families of focusing quadrupoles, one central quadrupole QF2 and two peripheral quadrupoles QF1 (see Fig. 1b). The gradients in the defocusing quadrupoles remain almost unchanged. The plus sign in (17) will correspond to the case where $\Delta G/G$ in the central quadrupole QF2 is about two times higher than in the other two quadrupoles QF1, which results in an unchanged frequency of betatron oscillations.

Numerical simulation of the magneto-optical lattice based on a three-cell superperiod with gradient modulation, which was carried out by the MAD code, yielded the following results. Figure 5 shows the calculated dependence of the transition energy $\gamma_{tr}$, horizontal $\beta_x$-function, horizontal dispersion $D_x$, and chromaticity $\xi_x$ normalized to $\nu$ on the horizontal betatron oscillation frequency $\nu$ normalized to $S$ for a superperiod consisting of three cells. A gradient modulation $\Delta G/G \approx 35\%$ proved to be necessary to obtain the zero momentum compaction factor at $\nu_{tr}/S = 3/4$ (i.e., at $\nu = \nu_{tr}$). Figure 6 shows the spectrum of Fourier harmonics of the modulated lens gradient function for this case, from which the harmonic amplitudes $g_1$ and $g_2$ can be found. Substituting these values into (17), we get an analytical dependence of the transition energy $\gamma_{tr}$ on $\nu/S$ (see Fig. 5). Here, in contrast with the case of orbit curvature modulation, two harmonics should be taken into account because the factor $1/[1-(1-kS/\nu)^2]^2$ in (15) increases the contribution from the second harmonic. A comparison of the numerical and analytical results (see Fig. 5) makes it possible to state that the resonant theory describes the properties of the lattice with gradient modulation quite satisfactorily.

To conclude the section, let us turn to the abovementioned KEK proton synchrotron [15] again and discuss whether it is possible to increase the transition energy by lens gradient modulation if a double superperiod is introduced in the ring. Note that the second har-

monic of the modulation function, dangerous in terms of excitation of the parametric resonance, is not necessarily present. Figure 7 shows the behavior of the parameters of the radial oscillation envelope and the dispersion in the unchanged lattice of the KEK proton synchrotron with double superperiod and gradient function modulation. The only possibility of obtaining the zero momentum compaction factor is to get zero mean dispersion because variation in curvature does not involve the required harmonic. To this end, it is necessary to make a rather close approach to the value $\nu/S = 1$, in this case for the shortened superperiod $\nu/S \approx 0.97$. Unfortunately, beginning with a certain modulation value, the contribution from the second harmonic ($k = 2$) becomes rather significant and an increase in the $\beta$-function is observed.

It is important that, although modulation of the gradient function may yield the required value of the momentum compaction factor, the ensuing excitation of the parametric resonance will cause an increase in the beam envelope leading to an increase in chromaticity and, as a result, to a decrease in the dynamic aperture. In addition, as is evident from Figs. 2 and 5, values of the $\beta$-function are almost a factor of 2 larger when the modulation of the gradient function is used to control lattice parameters. Yet, this method is more preferable for machines of older generation than the modulation of the orbit curvature function, because no changes in the accelerator design are required.

## 6. COMBINED MODULATION OF THE ORBIT CURVATURE FUNCTION AND THE LENS GRADIENT FUNCTION

Thus, modulation of the orbit curvature and modulation of the lens gradients can be used to obtain the required momentum compaction factor. The former method allows controlling the momentum compaction factor with the minimum increase in the $\beta_x$ function and $D_x$ and, compared with gradient modulation lattices, does not require strong sextupoles for chromaticity correction. However, the gradient modulation method is more flexible as it allows the momentum compaction factor of the already existing machine to be varied. In addition, it is often impossible to employ the factor $1/(kS/\nu - 1)$ and to increase it by making $\nu$ approach $kS$, which results in ineffectiveness of each method used separately. For example, in high-intensity accelerators one of the requirements is zero dispersion in straight sections. This means that the phase advance of radial oscillations in arcs should be a multiple of $2\pi$ and the condition $\min\{kS - \nu\} = 1$ should hold.

Based on the above reasoning, we developed a method of simultaneous orbit curvature and lens gradient modulation with an identical frequency of the fundamental harmonics and an approximately identical contribution to the final value of the momentum compaction factor.

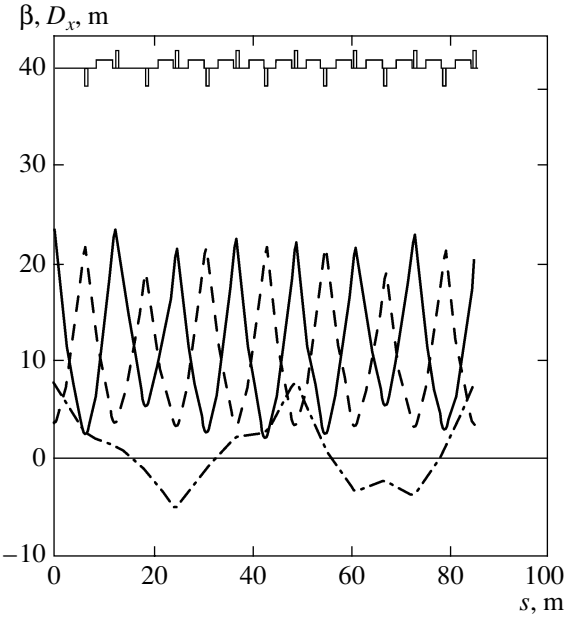


**Fig. 7.** Modified lattice of the KEK proton synchrotron: two superperiods with modulation of the gradient function (horizontal betatron frequency in the ring $\nu = 4 \times 1.9375$); designations of the curves are the same as in Fig. 1.

From (6) it is easy to derive the following equality for an arbitrary fundamental harmonic:

$$\left(\frac{\bar{R}}{\nu}\right)^2 \frac{g_k}{1-(1-kS/\nu)^2} - r_k = \pm 2\sqrt{\frac{kS}{\nu} - 1}. \qquad (19)$$

As was already mentioned, modulation of gradients and modulation of the orbit curvature should be in antiphase and the reasonable location of the missing magnet cell is at the center of the superperiod. This means that the amplitude of the fundamental harmonic of the orbit curvature modulation should be negative, $r_n < 0$. Then the amplitude of the gradient modulation will be positive, $g_k > 0$. As an example of a lattice with identical contributions from both modulations, we consider the adopted working version of the antiproton storage ring HESR [2, 3] consisting of two arcs and two straight sections (see Fig. 8). Each arc has a betatron frequency $\nu = 3$ and comprises four superperiods, i.e., $S = 4$.

To have equal contributions from both modulations to the final value of the momentum compaction factor, the missing magnet cell should be 1 m longer than the magnet cells. Figure 9 shows dependence of the momentum compaction factor $\alpha$, horizontal $\beta_x$-function, horizontal dispersion $D_x$, and horizontal chromaticity $\xi_x$ on the lens gradient modulation. Different scaling factors are introduced for the functions to show them all in one figure. When the missing magnet cell is 1 m longer than the regular cell (Fig. 9a), the zero momentum compaction factor is obtained only by a longer empty space at the center of the superperiod,

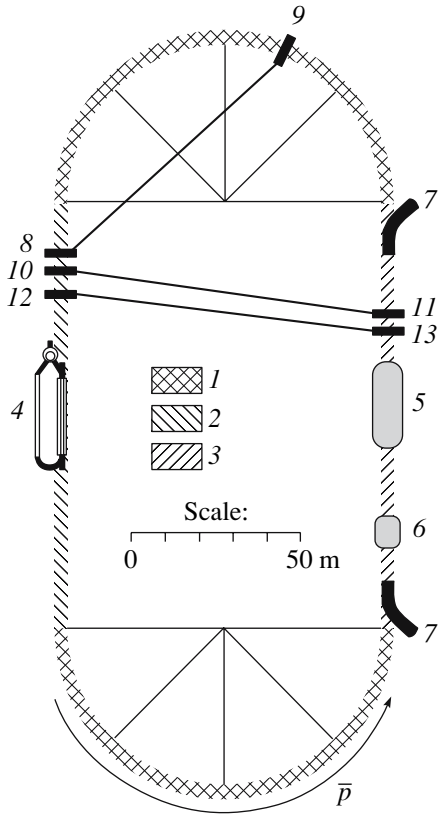


**Fig. 8.** Schematic view of the HESR: (*1*) superperiod (four superperiods in an arc); (*2*) straight section to accommodate electron cooling equipment; (*3*) straight section to accommodate experimental equipment; (*4*) electron cooling equipment; (*5*) experimental facility; (*6*) RF system; (*7*) septum in the longitudinal plane; (*8*) pickup and (*9*) kicker in the horizontal plane; (*10*) pickup and (*11*) kicker in the vertical plane; (*12*) pickup; (*13*) kicker.

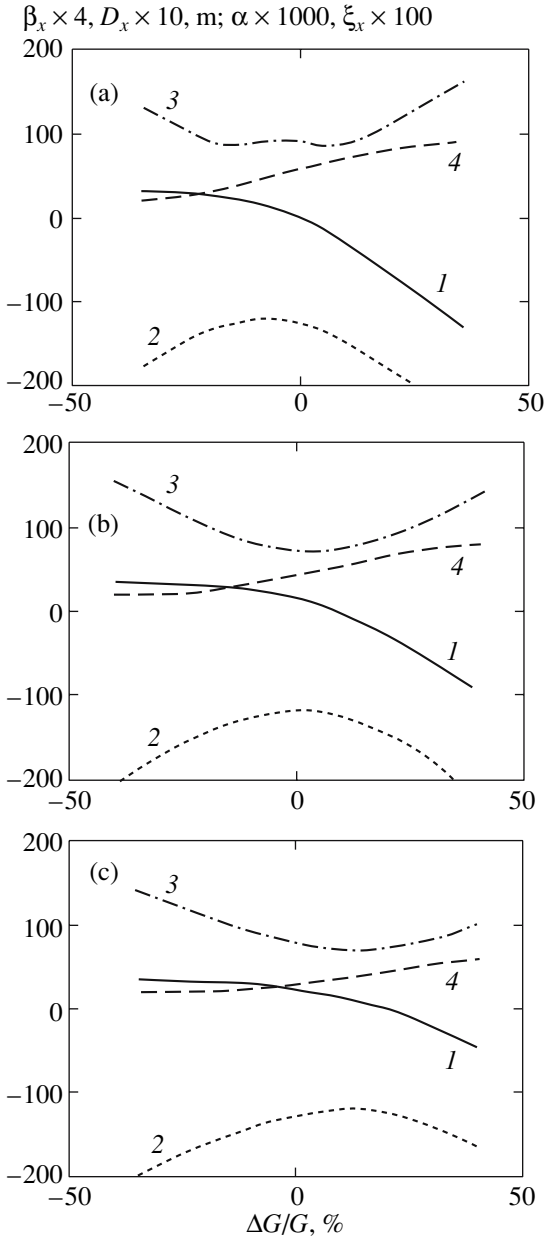


**Fig. 9.** Dependence of the functions $\alpha$ (*1*), $\xi_x$ (*2*), $\beta_x$ (*3*), and $D_x$ (*4*) on the gradient modulation when the missing magnet cell is 1 m longer than the regular cell (a), all cells are of equal length (b), and the missing magnet cell is 1 m shorter than the regular cell (c).

without modulation of gradients in quadrupole lenses. In this case gradient modulation is used to vary the momentum compaction factor as required within a wide range from $1/\nu^2$ to $-1/\nu^2$. When all cells are of equal length (Fig. 9b), the functions $\beta_x$, $D_x$, and $\xi_x$ are smoother and periodical due to more regular and periodical optics (no increase in their maximum values is observed). In this case, however, modulation of lens gradients at a level of approximately 5–10% is required in addition to modulation of the orbit curvature to obtain the zero momentum compaction factor. When the central cell is 1 m shorter than the regular cell (Fig. 9c), the zero momentum compaction factor can be obtained with additional modulation of gradients at a level of approximately 20%. Obviously, further decrease in the central cell length will entail larger and larger modulation of gradients and accordingly smaller and smaller spatial separation of the $\beta_{x,y}$-functions at the locations of the focusing and defocusing sextupoles. This in turn leads to a decrease in the efficiency of the sextupoles and thus to a decrease in the dynamic aperture.

The ultimate choice of the ratio between the contributions from two different modulations is sometimes dictated by the specifications and the requirement on the possible controlled variation range of the momentum compaction factor. In addition, the relation between the beam emittance and the momentum spread in the beam is important because it governs the limitations on the maximum values of the functions $\beta_x$, $D_x$, and $\xi_x$. The presented numerical results (Figs. 9a–9c) correspond to the complex transition energy $\gamma_{tr} = i5.5$.

Obviously, when the central cell length is varied within reasonable limits, all maximum characteristics of the dispersion and the envelope remain at practically the same level. Note, however, that an increase in the gradient modulation entails an increase in the maximum value of the gradient in the central lens.

## 7. MAGNETO-OPTICAL LATTICES OF ARCS AND STRAIGHT SECTIONS

Now let us consider the magneto-optical structure of the entire accelerator, i.e., lattices of its arcs and straight sections. Considering that physics equipment is to be installed in straight sections, let us formulate additional requirements on the resonant lattices:

(i) independent tuning of arcs and straight sections;

(ii) controllable variation of the momentum compaction factor within the range of $\alpha$ between $\sim 1/\nu^2$ and $\sim -1/\nu^2$;

(iii) ability to correct chromaticity of the entire accelerator by sextupoles located in the arcs;

(iv) a sufficiently large dynamic aperture with allowance for all nonlinearities;

(v) zero dispersion in straight sections.

The first condition determines the macrostructure of the accelerator, namely, separation in functions between arcs and straight sections. Arcs fulfill bending functions and functions governing the main magneto-optical characteristics of the lattice, such as the momentum compaction factor, suppression of chromaticity, zero dispersion in straight sections, and correction of higher-order nonlinearities. Straight sections fulfill functions associated with accommodation of experimental equipment and final tuning of betatron oscillation frequencies of the entire accelerator. In addition, the optics of the arcs should be independent of the optics of the straight sections to allow more convenient work and minimum preparation for experiments. The number of arcs and straight sections is dictated by many parameters, first of all by the required architecture of the ring and the projected experiments.

For the dispersion in straight sections to be zero, an arc consisting of $S_{arc}$ superperiods should have a phase advance of radial oscillations that is a multiple of $2\pi$; i.e., $\nu_{arc}$ should be an integer. This means that the phase advance in one superperiod should be $2\pi\nu_{arc}/S_{arc}$. On the other hand, for the momentum compaction factor to be controlled, the betatron frequency of horizontal oscillations should be smaller than the number of superperiods multiplied by the number of the fundamental harmonic. From this point of view it is reasonable to take the minimum possible difference

$$\nu_{arc} - kS_{arc} = -1.$$

Thus, there exist many ratios between $S_{arc}$ and $\nu_{arc}$:

$$(4:3), (6:5), (8:7), \ldots .$$

There is another possibility. The arc may be divided into an integral number of superperiods within which the above ratios hold. For example, in the J-PARC project, the ratio

$$S_{arc} : \nu_{arc} = 8:6$$

is chosen for the main ring [9, 10]. Actually, the arc is divided into two arcs in the ratio 4 : 3 without a straight section, and the zero dispersion condition is met not only at the edges but also in the middle of this double arc. As is seen, in all ratios the number of superperiods $S_{arc}$ is taken to be even while the betatron oscillation frequency $\nu_{arc}$ takes on integral odd values. In this case, the phase advance of the radial oscillations between the cells located in different superperiods and separated by $S_{arc}/2$ superperiods is obviously

$$\frac{\nu_{arc}}{S_{arc}}\frac{S_{arc}}{2} = \frac{\nu_{arc}}{2},$$

which corresponds to the condition of first-approximation mutual compensation of the nonlinear effects of sextupoles located in these cells. This remarkable property also applies to higher multipoles in bending magnets and quadrupoles because each of them has a partner in the other half of the arc at a distance of odd integral $\pi$ of radial oscillations.

Thus, choosing $S$, $k$, and $\nu$, we determine the lattice of the arc and the number of arcs. On the one hand, we are limited by strict rules for the choice of these parameters, and on the other, the choice is quite wide and we may speak about a certain class of accelerators with such arcs.

By way of example, let us consider two versions of the lattice for the HESR accelerator [2, 3] with an identical number of arcs and identical transition energy $\gamma_{tr} = i6$. In the first version, the arc has the number of superperiods $S_{arc} = 4$ and the frequency of radial oscillation in the arc $\nu_{arc} = 3$, in the second version $S_{arc} = 6$ and $\nu_{arc} = 5$. Figure 10 shows the $\beta$-functions and the dispersion along the lattice of the four- and six-superperiod arcs. For the dispersion in the straight sections to be zero, the phase advance of radial oscillations should be a multiple of $2\pi$ and the dispersion should begin with the zero value at the entrance of the arc. Therefore, the dispersion oscillates with a double frequency: the superperiod frequency and the arc periodicity (Figs. 10b, 10d). This leads to an additional increase in the maximum dispersion in the arc. For example, in the four-superperiod arc the dispersion increases from 5 to 6 m, which is a 20% increase, and in the six-superperiod arc the maximum dispersion increases from 4.5 to 6 m, which is a 30% increase. In the latter case the arc is longer and thus the arc periodicity causes a larger increase in dispersion. On the other hand, the six-superperiod arc has a shorter superperiod and thus smaller maximum values of the $\beta_{x,y}$-functions in comparison with the four-superperiod arc. Note that in both cases the arc periodicity of the dispersion function does not lead to variation in the

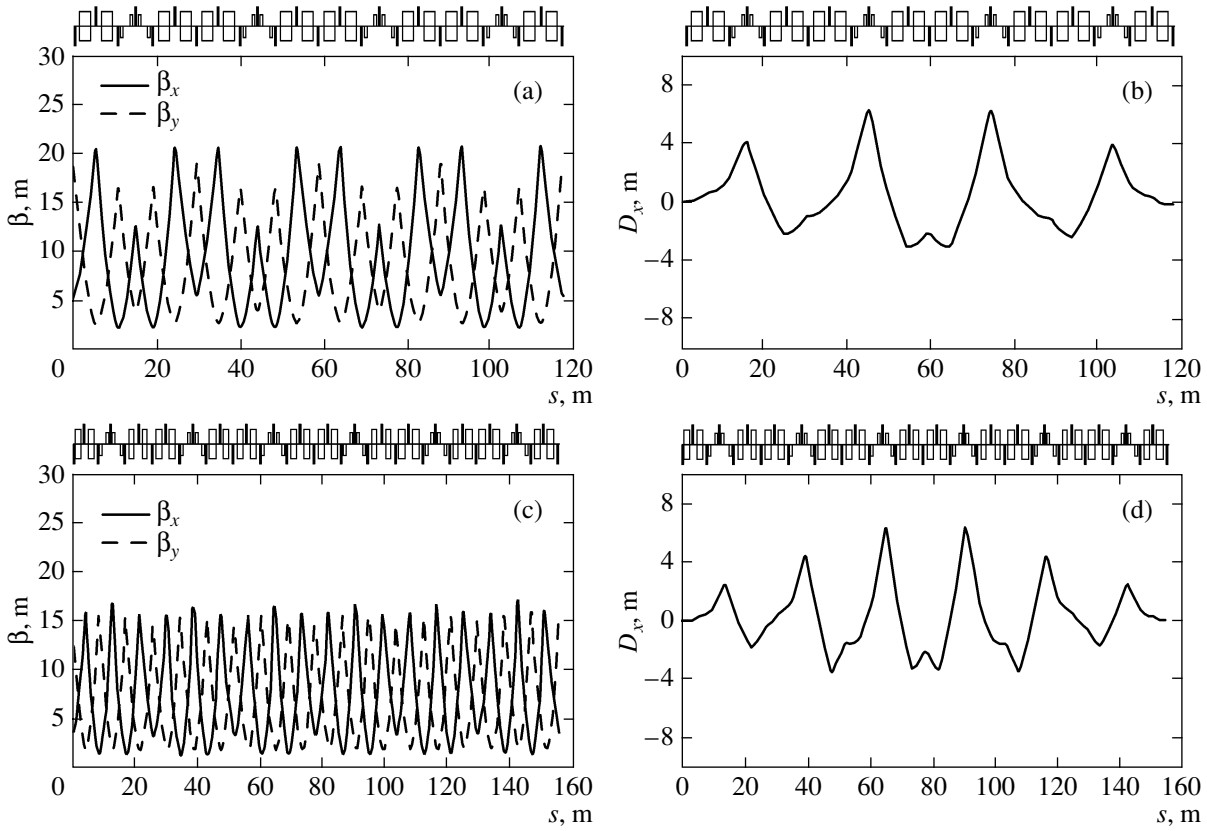


**Fig. 10.** Variation of β-function and dispersion along the magnetic structure in the four-superperiod arc (a, b) and the six-superperiod arc (c, d).

momentum compaction factor because integral (1) remains unchanged. The behavior of the $\beta_{x,y}$-functions also remains unchanged because the initial zero dispersion values do not affect them.

Since arcs and straight sections are separated in functions, the betatron oscillation frequencies $\nu_{x,y}$ in the arcs do not change in any mode of operation and therefore quadrupoles specially inserted in the straight sections and providing the desired fraction value of the betatron frequency of the entire machine are responsible for the control of the working point position. However, in the case of retuning of the momentum compaction factor, the arc edge values of the $\beta_{x,y}$-functions change. Therefore, special matching sections are inserted in the straight sections, which, with their four quadrupole lenses, allow matching of the arcs and straight sections to be retained. Figure 11a shows the behavior of the β-functions and the dispersion along the target-accommodating straight section of the HESR accelerator, which additionally includes a matching section with six lenses: four lenses for matching $\beta_{x,y}$-functions and two lenses for correcting betatron frequencies. As a result, arcs are fully independent of straight sections and correction of the momentum compaction factor does not affect the values of the $\beta_{x,y}$-functions set for the experiments.

If there are no special requirements on the behavior of the $\beta_{x,y}$-functions in the straight sections, the straight section lattice is usually mirror symmetrical about its middle, and therefore all lenses of the straight sections can be directly used for matching arcs and straight sections. This considerably simplifies tuning of the entire accelerator due to minimization of the number of quadrupole families in the straight sections. By way of example, Fig. 11b shows the behavior of the β-functions and the dispersion along the magneto-optical lattice of the arc and the straight section for a 3-GeV accelerator. The straight section has seven quadrupoles (four families) and allows easy matching of the arc and the straight section.

## 8. CONTROL OF THE MOMENTUM COMPACTION FACTOR AND THE BETATRON FREQUENCIES

To control and vary the momentum compaction factor, it is reasonable to use only modulation of gradients in quadrupoles of arcs at a fixed orbit curvature modulation. Adopting this scheme, we should know which elements are directly responsible for adjustment of the momentum compaction factor and for tuning of frequencies in both planes. In addition, it is necessary to learn to what extent they affect one another while each of the parameters is being varied. Special properties of

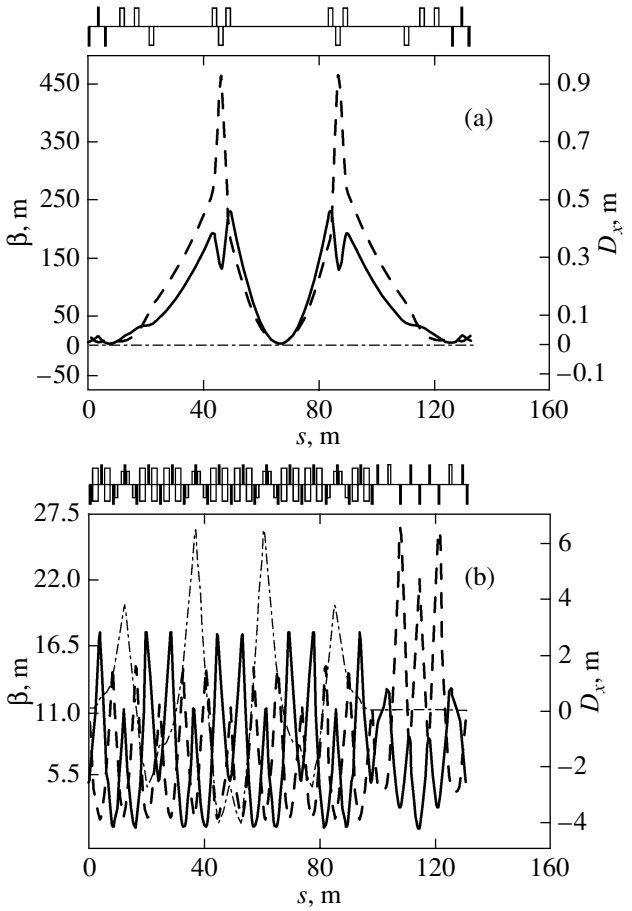


**Fig. 11.** Behavior of the β-functions and dispersion along the target-housing straight section in the HESR (a) and along the half-lattice of the accelerator (arc and straight section) without special matching section (b); designations of the curves are the same as in Fig. 1.

the resonant lattice allow independent control of each parameter mentioned. According to [1], in the case of a mirror-symmetrical superperiod the dispersion function and the horizontal β-function vary along the superperiod in the following way:

$$D(\phi) \propto 1 - \frac{1}{2}\left(\frac{\bar{R}}{\nu}\right)^2 \times \frac{g_k \cos k\phi}{(1 - kS/\nu)[1 - (1 - kS/\nu)^2]} + \frac{1}{2}\frac{r_k \cos k\phi}{1 - kS/\nu}, \quad (20)$$

$$\beta_x \propto \cos\mu\phi\left[1 - \frac{1}{2}\left(\frac{\bar{R}}{\nu}\right)^2 g_k \frac{\cos k\phi}{1 - (1 - kS/\nu)^2}\right].$$

When $kS > \nu$, $g_k > 0$, and $r_k < 0$, the maximum of the dispersion is at the center of the superperiod, namely, at the point $\phi = 0$ and the maximum of the horizontal β-function is at the edges of the superperiod at the points $\phi = -\pi$ and $\phi = \pi$ (see Figs. 10a, 10b). With thus

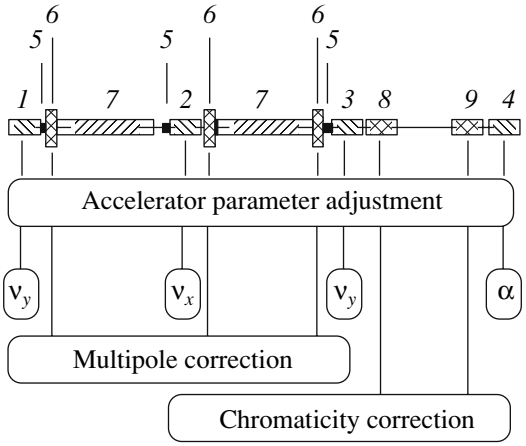


**Fig. 12.** Accelerator parameter control schematically illustrated by the example of a half-superperiod. Quadrupoles: (*1*) QD1 or QD, (*2*) QF1, (*3*) QD2 or QD, (*4*) QF2; (*5*) beam monitors; (*6*) multipole correctors; (*7*) bending magnets; sextupoles (*8*) SD, (*9*) SF (F and D denote focusing or defocusing family, respectively).

separated maxima of these functions, we create conditions for independent control over the betatron frequency and the momentum compaction factor. The accelerator parameter control is diagrammatically shown in Fig. 12. In the resonant lattice the central focusing quadrupole QF2 is placed at the point of the maximum dispersion and thus has a dominant role in its variation and control over the transition energy. The other focusing quadrupole QF1 is placed at the point of the $\beta_x$-function maximum, which makes it utterly effective for controlling the frequency of horizontal betatron oscillations. Due to the properties of the FODO lattice, the $\beta_{x,y}$-functions in both planes are quite well separated and can independently affect frequencies in different planes. To prove that the momentum compaction factor and the betatron frequencies are controlled independently, we numerically simulated these processes for the HESR accelerator lattice with the initially taken momentum compaction factor $\alpha = -0.02$ ($\gamma_{tr} \approx i7$).

Figure 13a shows how the function of gradients in the quadrupoles QF1, QF2, QD1, QD2, or QD (with one family of defocusing lenses QD1-QD2) affects the momentum compaction factor in the vicinity of the value $\alpha = -0.02$. The results presented in the figure allow the conclusion that

$$\frac{\partial\alpha}{\partial G_{QF2}} \gg \frac{\partial\alpha}{\partial G_{QF1}} \approx \frac{\partial\alpha}{\partial G_{QD1}} \approx \frac{\partial\alpha}{\partial G_{QD2}}. \quad (21)$$

Thus, the momentum compaction factor is well controlled by the central quadrupole QF2 and practically does not depend on the gradients in the other quadrupoles. Figures 13b and 13c show numerically simulated variations in the frequencies of horizontal and vertical betatron oscillations in arcs under the effect of various quadrupole families in the vicinity of the working point

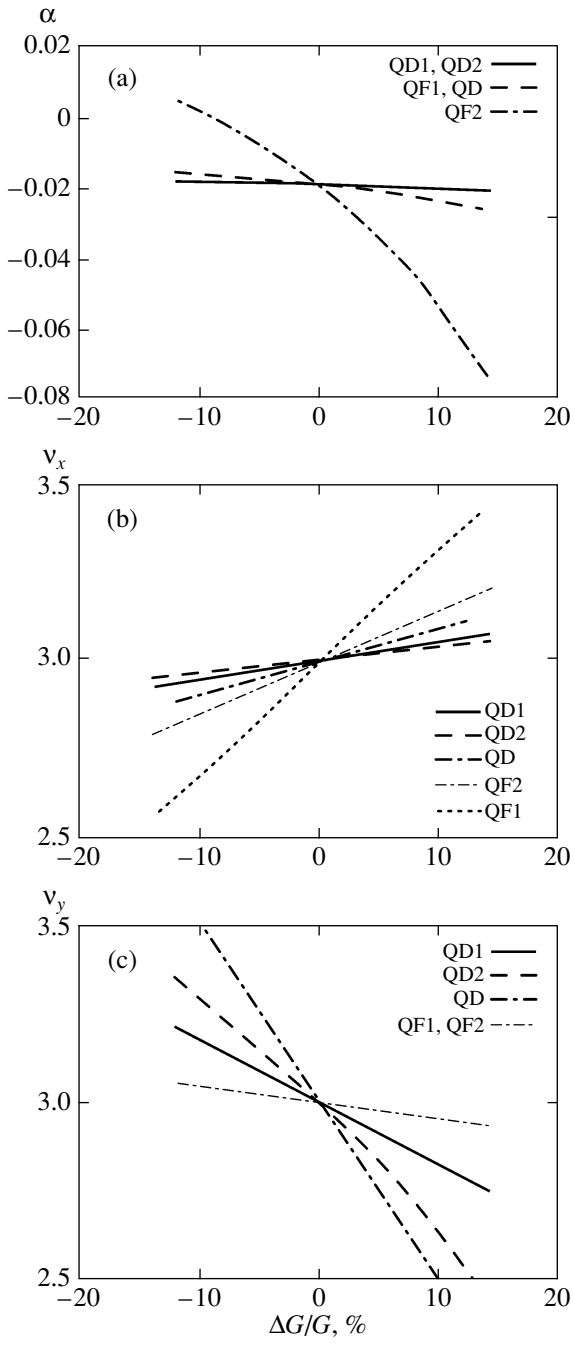


**Fig. 13.** Dependence of the momentum compaction factor (a) and the horizontal (b) and vertical (c) frequencies in the arcs on the gradients in the quadrupoles.

of the frequencies $\nu_x = 3.0$ and $\nu_y = 3.0$. It is evident that the derivatives of the horizontal and vertical frequencies with respect to the gradients in different lenses have different values. For example, the horizontal frequency is most sensitive to gradients in the family of lenses QF1, less sensitive to lenses QF2, and practically insensitive to defocusing lenses. The vertical frequency is equally strongly affected by the families of lenses QD1 and QD2, while the focusing quadrupole families practically do not affect it. These results allow the following conclusion:

$$\begin{aligned}\frac{\partial \nu_x}{\partial G_{\mathrm{QF1}}} &> \frac{\partial \nu_x}{\partial G_{\mathrm{QF2}}} \gg \frac{\partial \nu_x}{\partial G_{\mathrm{QD1}}} \approx \frac{\partial \nu_x}{\partial G_{\mathrm{QD2}}},\\ \frac{\partial \nu_y}{\partial G_{\mathrm{QD1}}} &\approx \frac{\partial \nu_y}{\partial G_{\mathrm{QD2}}} \gg \frac{\partial \nu_y}{\partial G_{\mathrm{QF1}}} \approx \frac{\partial \nu_y}{\partial G_{\mathrm{QF2}}}.\end{aligned} \tag{22}$$

Since lenses QD1 and QD2 identically affect all accelerator parameters, it is reasonable to reduce the number of families of defocusing quadrupoles QD1 and QD2 to one QD family.

Thus, using numerical simulation, we have proved that the betatron frequencies and the momentum compaction factor are controlled separately. It has been revealed that

(i) the momentum compaction factor is controlled by the family of quadrupoles QF2;

(ii) the horizontal frequency is tuned by the family of quadrupoles QF1;

(iii) the vertical frequency is tuned by the family of quadrupoles QD1 and QD2 or QD.

## 9. CORRECTION AND COMPENSATION OF CHROMATICITY

Chromaticity arises from dependence of the focusing properties of quadrupoles on the particle momentum and is governed by the derivative

$$Q'_{x,y} = \frac{d\nu_{x,y}}{d\delta},$$

where $\delta = \Delta p/p$ is the momentum spread. Two families of sextupoles (focusing, SF, and defocusing, SD) are used to correct chromaticity. Their integral effect in the horizontal and vertical planes is defined by the expression

$$\frac{\partial \nu_{x,y}}{\partial \delta} = \pm\frac{1}{4\pi}\int_0^C \beta_{x,y}(s)D(s)S(s)ds. \tag{23}$$

Obviously, sextupoles of each family should be located at the places of the maximum values of the dispersion and $\beta_{x,y}$-functions for more effective correction of chromaticity. In this connection, the resonant lattice based on FODO cells is most convenient as compared with doublet and triplet lattices because in the resonant lattice the behavior of the $\beta_{x,y}$-functions is different and their maxima are separated and the dispersion in each of the maxima is quite large. In addition, as we already mentioned, the resonant lattice comprises empty cells where sextupoles can be most effectively placed (see Fig. 1). As a result, the number of sextupole families intended for chromaticity correction in the resonant lattice is the smallest possible: one focusing family and one defocusing family. Thus, the main requirement on the sextupoles is the possibility of relatively indepen-

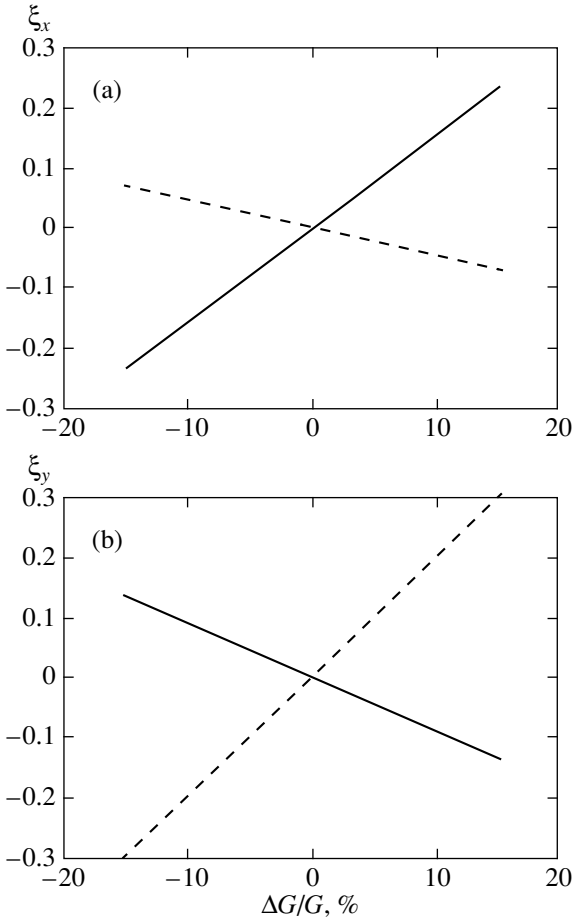


**Fig. 14.** Dependence of the horizontal (a) and vertical (b) chromaticity on the gradients in the focusing (SF, solid lines) and defocusing (SD, dashed lines) sextupole families.

dent correction in both planes simultaneously. To prove the correctness of the chosen locations of sextupoles, we numerically simulated correction of chromaticity to the zero value $\xi_{x,y} = 0$ using the HESR accelerator lattice as an example. Figure 15 shows the resulting dependences of the horizontal and vertical chromaticity on the gradients in the focusing (SF) and defocusing (SD) sextupoles. It is evident from the results presented in the figures that derivatives of chromaticity with respect to gradients in sextupoles meet the conditions

$$\left|\frac{\partial \xi_x}{\partial G_{\mathrm{SF}}}\right| > \left|\frac{\partial \xi_x}{\partial G_{\mathrm{SD}}}\right|, \quad \left|\frac{\partial \xi_y}{\partial G_{\mathrm{SD}}}\right| > \left|\frac{\partial \xi_y}{\partial G_{\mathrm{SF}}}\right|. \tag{24}$$

Thus, the conclusion may be drawn that both sextupole families effectively control chromaticity in both planes independently of each other.

## 10. CONCLUSIONS

A general approach to constructing a resonant magneto-optical lattice on the basis of correlated and resonant modulation of the lens gradient and orbit curvature functions is presented in the paper. The developed resonant lattice makes it possible to vary the momentum compaction factor in a wide range and eliminate crossing of the transition energy by accelerated particles. The basis for this lattice is the FODO cell, best suitable for independent control of the betatron oscillation frequencies and the momentum compaction factor. Various methods for control of the momentum compaction factor are considered, which resulted in the optimum magneto-optical lattice. It provides mutual compensation of the nonlinear effects of the chromatic sextupoles and higher multipoles of the lattice and has zero dispersion in the straight sections. The effective system for correction of chromaticity by a minimum number of sextupole families allows the largest possible dynamic aperture. The research has resulted in the acceptance of this type of lattice as the basic one for the HESR storage ring, which is part of the international FAIR project. This lattice meets all requirements of the physics experiments planned at this facility. Apart from the HESR, the resonant lattice has also found application at other international facilities, in particular at the J-PARC main ring under construction.

## REFERENCES

1. Yu. V. Senichev and A. N. Chechenin, Zh. Éksp. Teor. Fiz. **132**, 1127 (2007) [JETP **105**, 988 (2007)].
2. Yu. Senichev, in *Proceedings of 33rd ICFA* (Bensheim, Darmstadt, Germany, 2004), p. 443.
3. Yu. Senichev et al., in *Proceedings of European Particle Accelerator Conference* (Lucerne, 2004), p. 653; http://accelconf.web.cern.ch/accelconf/e04/papers/moplt047.pdf.
4. Yu. Senichev, in *Proceedings of XI Meeting of International Collaboration on Advanced Neutron Sources* (KEK, Tsukuba, 1990); Yu. Senichev et al., in *IEEE Proceedings of Particle Accelerator Conference* (San Francisco, CA, 1991), p. 2823; http://accelconf.web.cern.ch/accelconf/p91/pdf/pac1991_2823.pdf.
5. M. Craddock, in *IEEE Proceedings of Particle Accelerator Conference* (San Francisco, CA, 1991), p. 57; http://accelconf.web.cern.ch/accelconf/p91/pdf/pac1991_0057.pdf.
6. U. Wienands, N. Golubeva, A. Iliev, et al., in *Proceedings of XV International Conference on High Energy Accelerators* (Hamburg, Germany, 1992), p. 1073.
7. E. Courant, A. Garen, and U. Wienands, in *Proceedings of IEEE Particle Accelerator Conference* (San Francisco, CA, 1991), p. 2829, http://accelconf.web.cern.ch/accelconf/p91/pdf/pac1991_2829.pdf.
8. H. Schönauer, B. Autin, R. Cappi, et al., in *Proceedings of IEEE European Particle Accelerator Conference* (Vienna, 2000), p. 966; http://accelconf.web.cern.ch/accelconf/e00/papers/thp2A09.pdf.
9. Y. Mori, ICFA Beam Dyn. Newsl., No. 11, 12 (1996); http://icfausa.jlab.org/archive/newsletter/icfa_bd_nl_11.pdf.

10. Y. Ishi, S. Machida, Y. Mori, and S. Shibuya, in *Proceedings of Second Asia Particle Accelerator Conference, APAC'01, Beijing, China, 2001* (2002); http://hadron.kek.jp/jhf/apac98/5d002.pdf.

11. H. Bruck, in *Proceedings of IX International Conference on High Energy Accelerator* (SLAC, Stanford, CA, 1974), p. 615.

12. R. Gupta, J. Botman, and M. Craddock, IEEE Trans. Nucl. Sci. **32**, 2308 (1985); http://accelconf.web.cern.ch/accelconf/p85/pdf/pac1985_2308.pdf.

13. H. Grote and F. C. Iselin, The MAD Program, User's Reference Manual (CERN, 1995), SL Note 90-13 (AP), Rev. 4; http://hansg.web.cern.ch/hansg/mad/mad8/user/mad.html.

14. V. Lebedev, OptiM—Computer Code for Linear and Non-Linear Optics Calculations; http://www-bdnew.fnal.gov/pbar/organizationalchart/lebedev/OptiM/optim.htm.

15. T. Suzuki, KEK-Reports, KEK-74-4 (1974).

*Translated by M. Potapov*